Scalar-gauge dynamics in (2+1) dimensions at small and large scalar couplings

O. Philipsen[1], M. Teper[2] and H. Wittig[2,*]

[1] *Theoretische Physik, Universität Heidelberg*

Philosophenweg 16, D-69120 Heidelberg, Germany

[2] *Theoretical Physics, University of Oxford*

1 Keble Road, Oxford OX1 3NP, U.K.

Abstract

We present the results of a detailed calculation of the excitation spectrum of states with quantum numbers $J^{PC} = 0^{++}, 1^{--}$ and 2^{++} in the three-dimensional SU(2) Higgs model at two values of the scalar self-coupling and for fixed gauge coupling. In the context of studies of the electroweak phase transition at finite temperature these couplings correspond to tree-level, zero temperature Higgs masses of $35 \, \mathrm{GeV}$ and $120 \, \mathrm{GeV}$, respectively. We also study the properties of Polyakov loop operators, which serve to test the confining properties of the model in the symmetric phase. At both values of the scalar coupling we obtain masses of bound states consisting entirely of gauge degrees of freedom ("W-balls"), which are very close to those obtained in the pure gauge theory. We conclude that the previously observed, approximate decoupling of the scalar and gauge sectors of the theory persists at large scalar couplings. We study the crossover region at large scalar coupling and present a scenario how the confining properties of the model in the symmetric phase are lost inside the crossover by means of flux tube decay. We conclude that the underlying dynamics responsible for the observed dense spectrum of states in the Higgs region at large couplings must be different from that in the symmetric phase.

---

1 Introduction

Over the past few years the SU(2) Higgs model in three dimensions has been the subject of many thorough numerical studies by means of lattice Monte Carlo simulations [1] – [5]. The main incentive for these investigations was to clarify the nature of the electroweak phase transition in the framework of the dimensional reduction programme [6], where it is much easier to obtain precise numerical results than in the full four-dimensional theory at finite temperature [7]. In these studies it has been established that the electroweak phase transition is weakly first order for Higgs masses up to $m_H \sim 70\,\mathrm{GeV}$, while for Higgs masses $m_H \gtrsim 80\,\mathrm{GeV}$ the transition disappears and turns into a smooth crossover [8, 2]. Hence, the Higgs region and the confinement region in parameter space are indeed analytically connected, as was conjectured a long time ago for models with fixed-length Higgs fields [9]. A review of the existing lattice results as well as a comparison with perturbation theory can be found in [10].

While the nature of the phase diagram and the order of the phase transition are now well determined, our understanding of the symmetric phase is still incomplete. Calculations of the mass spectrum based on the use of gauge-invariant operators lead to a picture of a confining symmetric phase with a dense spectrum of bound states. Recent attempts to describe the spectrum in terms of bound state models may be found in [11, 12]. This part of the phase diagram is of great intrinsic interest because it exhibits the same qualitative behaviour as QCD. In this region the non-abelian gauge theory has confining properties, but confinement is not exact due to the presence of matter fields in the fundamental representation, which lead eventually to the screening of charges at large distances. This apparent similarity between QCD and the symmetric phase of scalar-gauge models opens the possibility to study some aspects of QCD in a model that is computationally much less demanding.

In the Higgs phase, on the other hand, for small enough scalar couplings a perturbative calculation of the spectrum is applicable and leads to results in good agreement with those from lattice simulations. Due to the analytic connectedness of the phase diagram all mass eigenstates in the Higgs region may be continuously mapped into their counterparts in the confinement region. This offers the possibility to study the onset of non-perturbative physics and confinement by smoothly moving from the Higgs region into the confinement region of the phase diagram.

In this paper we elaborate on our previous computation of the mass spectrum of the SU(2) Higgs model in 2+1 dimensions [4]. Here, however, we deviate somewhat from the

original context of the electroweak phase transition, since our main interest lies in the dynamics of this theory and what it might have in common with QCD. In particular, we want to obtain a more complete picture of the excitation spectrum and investigate in more detail the previously observed approximate decoupling of the scalar and gauge sectors of the model [4]. Thus, in addition to the 0^{++} and 1^{--} states considered before, we now also compute correlations of 2^{++} and Polyakov loop operators. Although our analysis does not yet incorporate multiparticle states, it leads to a more complete picture of the symmetric phase.

In contrast to our previous work, where we carefully studied the approach to the continuum limit, we now consider the theory at a fixed value of the gauge coupling, i.e. $\beta_G = 9$, where our earlier results show that the physics is already very close to the continuum limit.

Our main results are as follows. The previously observed approximate decoupling of states composed purely out of gauge degrees of freedom in the 0^{++} channel [4] extends to the 2^{++} channel. The masses of these states are very close to their values in the pure gauge theory. Furthermore, the decoupling occurs at both small and large values of the scalar self-coupling, and in the latter case it can be observed also deep in the crossover region. Second, at large scalar coupling we find that a dense spectrum of states is observed even in the Higgs phase, yet the underlying dynamics must be quite different, as confinement is no longer observed. We present a scenario how the confining properties of the theory are lost inside the crossover region: within the QCD context it is natural to use the concept of flux tubes in the symmetric phase as a manifestation of confinement. As one enters the crossover region the flux tube develops a rapidly growing decay width and eventually becomes so unstable that confinement is lost entirely. Finally, the inclusion of correlations of Polyakov loops changes some of our previous conclusions about the influence of finite-volume effects. In particular, we find that finite-size effects, especially in the lowest 0^{++} state are less severe than was claimed before [4].

Some of the results presented in this paper have been summarised elsewhere [13, 14]. We also draw the reader's attention to some recent related work [15].

The remainder of this paper is organised as follows. In section 2 we briefly summarise the lattice techniques used in this work. Section 3 contains a discussion and comparison of the properties of the Higgs and confinement phases for small scalar self-coupling. In section 4 we describe how the properties of the Higgs and confinement regions of the phase diagram change when the size of the scalar self-coupling is increased. In section 5 we follow the analytic connection of the mass spectrum through the crossover. Results

indicating flux tube decay in the crossover region are presented in section 6, and section 7 contains our conclusions.

2 Methodology

We work with the three-dimensional lattice action given by

$$
\begin{aligned}
S[U,\phi] \;=\; & \beta_G \sum_p \left(1 - \frac{1}{2}\mathrm{Tr}U_p\right) + \sum_x \left\{ - \beta_H \sum_{\mu=1}^{3} \frac{1}{2}\mathrm{Tr}\Big(\phi^\dagger(x)U_\mu(x)\phi(x+\hat{\mu})\Big) \right. \\
& \left. + \frac{1}{2}\mathrm{Tr}\Big(\phi^\dagger(x)\phi(x)\Big) + \beta_R \left[\frac{1}{2}\mathrm{Tr}\Big(\phi^\dagger(x)\phi(x)\Big) - 1\right]^2 \right\},
\end{aligned}
\tag{1}
$$

where $U_\mu(x) \in \mathrm{SU}(2)$ is the link variable, U_p denotes the plaquette, and $\phi(x)$ is the scalar field. The bare parameters β_G, β_H and β_R are the inverse gauge coupling, the scalar hopping parameter, and scalar self-coupling, respectively. In our simulations we fix the combination of parameters

$$
\frac{\lambda_3}{g_3^2} = \frac{\beta_R\,\beta_G}{\beta_H^2} \;,
\tag{2}
$$

where λ_3/g_3^2 is the ratio of the scalar self-coupling and the gauge coupling in the continuum formulation. Exact relations between the lattice and the continuum parameters at the two-loop level governing the approach to the continuum limit can be found in [16]. In this work we consider the cases of small, i.e. $\lambda_3 \ll g_3^2$ and large, i.e. $\lambda_3 \sim O(g_3^2)$ scalar self-coupling, by choosing $\lambda_3/g_3^2 = 0.0239$ and $\lambda_3/g_3^2 = 0.2743$, respectively. At tree level, this ratio is proportional to the ratio of Higgs and W-boson masses. As an orientation for those readers who are familiar with studies of the electroweak phase transition, we add that in the framework of dimensional reduction, our values of λ_3/g_3^2 correspond to tree-level, zero temperature Higgs masses of 35 GeV and 120 GeV, respectively [1].

2.1 The blocking procedure

In any mass calculation on the lattice it is important to have a good projection property of the interpolating operators in order to obtain a reliable signal. For gauge theories with or without scalar fields it has been demonstrated that the projection of the basic operators onto the desired state can be considerably enhanced by employing so-called "blocking" or "fuzzing" techniques [17, 18, 19, 4].

As in our previous work [4], we construct blocked link variables $U_\mu^{(n)}(x)$ at blocking level n according to the procedure originally defined in [17]. Furthermore, a blocked

version of the scalar field, $\phi^{(n)}(x)$ at blocking level n is constructed according to

$$\phi^{(n)}(x) = \frac{1}{5}\left\{\phi^{(n-1)}(x) + \sum_{j=1}^{2}\left[U_j^{(n-1)}(x)\phi^{(n-1)}(x+\hat{\jmath}) + U_j^{(n-1)\dagger}(x-\hat{\jmath})\phi^{(n-1)}(x-\hat{\jmath})\right]\right\}.$$
(3)

Note that we will take correlations in the $\hat{3}$ direction and so our blocking always remains within the $(1,2)$-plane. In addition, we consider blocked scalar fields $\phi^{(n,j)}(x)$ with non-local contributions from one spatial direction j only:

$$\phi^{(n,j)}(x) = \frac{1}{3}\Big\{\phi^{(n-1,j)}(x) \;\; + \;\; U_j^{(n-1)}(x)\phi^{(n-1,j)}(x+\hat{\jmath})$$
$$+ \;\; U_j^{(n-1)\dagger}(x-\hat{\jmath})\phi^{(n-1,j)}(x-\hat{\jmath})\Big\}, \quad j = 1, 2.$$
(4)

It is obvious that all blocking procedures employed are gauge invariant and can be iterated in order to create a large set of operators of various spatial extensions in an efficient manner. In practice, the blocking levels have to be tuned in order to identify the operators with the best projection properties.

2.2 Basic operators

We now proceed to list the basic operators used in our simulation. Since we use a larger set of operators compared to our previous calculation, we have decided to change our notation slightly for clarity. Although in general we use blocked links and scalar fields, we suppress the superscripts which label the blocking level in this subsection, except when stated explicitly.

After decomposing the scalar field $\phi(x)$ as

$$\phi(x) = \rho(x)\alpha(x), \quad \rho(x) \geq 0, \quad \alpha(x) \in \mathrm{SU}(2),$$
(5)

we consider the following basic operators involving only scalar fields or combinations of scalar and gauge degrees of freedom:

$$R(x) \;\; \equiv \;\; \frac{1}{2}\mathrm{Tr}\left(\phi^\dagger(x)\phi(x)\right),$$
$$L_j(x) \;\; \equiv \;\; \frac{1}{2}\mathrm{Tr}\left(\alpha^\dagger(x)U_j(x)\alpha(x+\hat{\jmath})\right), \quad j = 1, 2$$
$$V_j^a(x) \;\; \equiv \;\; \frac{1}{2}\mathrm{Tr}\left(\tau^a\alpha^\dagger(x)U_j(x)\alpha(x+\hat{\jmath})\right), \quad j = 1, 2,$$
(6)

where τ^a is a Pauli matrix. Note that at this stage we have not yet specified the quantum numbers J^{PC} of the operators. This is postponed to the end of this subsection when all basic operators have already been defined.

We also consider operators constructed out of link variables only, e.g.

$$C_{ij}^{1\times1}(x) = \text{Tr}\left(U_i(x)U_j(x+\hat{\imath})U_i^\dagger(x+\hat{\jmath})U_j^\dagger(x)\right), \quad i,j=1,2, \ i\neq j, \tag{7}$$

and in addition to the elementary plaquette $C^{1\times1}$, we also consider squares of size 2×2 as well as rectangles of size 1×2, 1×3, 2×3. Hence, we have five versions of operators consisting of closed loops of gauge fields, viz.

$$C_{ij}^{1\times1}, \ C_{ij}^{2\times2}, \ C_{ij}^{1\times2}, \ C_{ij}^{1\times3}, \ C_{ij}^{2\times3}. \tag{8}$$

As we shall see, a larger set of this type of operator will significantly improve our ability to extract information about the gauge sector of the theory.

An operator which is useful to probe the confining properties of a theory is the Polyakov loop, i.e. a loop of length L of link variables that winds around the spatial dimensions of the lattice, viz.

$$P_j^{(L)}(x) = \text{Tr}\prod_{m=0}^{L-1} U_j(x+m\hat{\jmath}), \quad j=1,2. \tag{9}$$

The expectation value of the Polyakov loop vanishes if the theory is confining, and it projects onto the state consisting of a chromoelectric flux loop that closes through the boundary in the $\hat{\jmath}$ direction. Correlations of $P_j^{(L)}$ can then be used to extract a string tension from the lowest mode of its exponential fall-off, the so-called "torelon" mass. However, in a theory with matter fields, such as ours, one eventually expects the string to break beyond some large separation, due to pair creation (just as in QCD). In our model we also have a phase with spontaneously broken symmetry, the Higgs phase. Here, this interpretation of the Polyakov loop correlator no longer holds, the Polyakov loop has a large expectation value, and the torelon mass cannot be used to extract a string tension. Instead, if a weak coupling expansion of the Polyakov loop correlator applies, its leading term corresponds to an exchange of two spin-1 particles (i.e. the W-boson), and therefore the lightest mass above the vacuum should be interpreted as a two-W state.

Apart from being relevant for the study of confinement, the Polyakov loop also plays an important rôle in understanding apparent finite-size effects in glueball calculations [20]. Since we are interested in the detailed structure of the spectrum, and, in particular, higher excitations, we need to address the influence of torelons in the various spin channels. Although single torelons, arising from correlations of the Polyakov loop $P_j^{(L)}$ cannot contribute directly to correlations of operators $C^{1\times1},\ldots,C^{2\times3}$ if confinement is exact, they may well be relevant for the operators $R(x)$ and $L_j(x)$. This is because

of the iterative, non-local nature of the blocking procedure, such that highly blocked versions of $R(x)$ and $L_j(x)$ may accidentally contain contributions which, for periodic boundary conditions, wind around the lattice and may thus have a sizeable projection onto $P_j^{(L)}$. Furthermore, torelon-antitorelon pairs are known to give rise to large finite-volume effects in glueball calculations [20]. Apart from studying correlations of Polyakov loops *per se*, we have decided to construct single-torelon and torelon-pair operators in the 0^{++} and 2^{++} channels and to study their correlations as a safeguard against finite-size effects.

We now give a complete list of the types of operators with quantum numbers J^{PC} and also introduce the symbols which will later label the contributions from the various operators to a given state.

0^{++} channel:

R: $R(x)$

L: $L_1(x) + L_2(x)$

C: symmetric combinations of $C^{1\times1}$, $C^{2\times2}$, $C^{1\times2}$, $C^{1\times3}$, $C^{2\times3}$

P: $P_1^{(L)}(x) + P_2^{(L)}(x)$

P_d: $P_1^{(L)}(x) \cdot P_2^{(L)}(x)$

T: $\left(P_1^{(L)}(x)\right)^2 + \left(P_2^{(L)}(x)\right)^2$

1^{--} channel:

V: $V_j^a(x)$, $j = 1, 2$ $a = 1, 2, 3$

2^{++} channel:

R: $R_-^{(n)}(x) \equiv \frac{1}{2}\left\{\mathrm{Tr}[\phi^{(n,1)\dagger}(x)\phi^{(n,1)}(x)] - \mathrm{Tr}[\phi^{(n,2)\dagger}(x)\phi^{(n,2)}(x)]\right\}$, $n > 1$

L: $L_1(x) - L_2(x)$

C: antisymmetric combinations of $C^{1\times2}$, $C^{1\times3}$, $C^{2\times3}$

P: $P_1^{(L)}(x) - P_2^{(L)}(x)$

T: $\left(P_1^{(L)}(x)\right)^2 - \left(P_2^{(L)}(x)\right)^2$

Here, the labels R, L refer to scalar operators, whereas C-type operators are composed only out of gauge degrees of freedom. The labels P, P_d denote torelon operators, and T labels pairs of torelons in the respective channels. Note that the definition of the operator $R_-^{(n)}$ in the 2^{++} channel is only possible with the kind of blocking defined in eq. (4).

Our list of operators does not contain multiparticle operators, and therefore we do

not have control over continuum states in the spectrum[2]. Here we wish to remark that we have evidence that continuum states have only small overlaps on the basis of operators used in this work, so that we are still able to extract the bound state mass spectrum reliably.

2.3   Matrix correlators

In order to compute the excitation spectrum of states with given quantum numbers, we construct matrix correlators by measuring all cross correlations between different types of operators at several blocking levels [4]. This correlation matrix can then be diagonalised numerically following a variational method. For a given set of N operators ϕ_i we find the linear combination that minimises the energy, corresponding to the lightest state.

The first excitation can be found by applying the same procedure to the subspace $\{\phi_i\}'$ which is orthogonal to the ground state. This may be continued to higher states so that we end up with a set of N eigenstates Φ_i, $i = 1, \ldots, N$ given by

$$\Phi_i = \sum_{k=1}^{N} a_{ik} \phi_k. \tag{10}$$

The coefficients a_{ik} quantify the overlap of each individual operator ϕ_k used in the simulation onto a particular approximate mass eigenstate Φ_i. For a complete basis of operators this procedure is exact. In practice, the quality of the approximation clearly depends on the number N of original operators and their projection properties. The determined eigenstates are removed from the basis for the higher excitations, so that the basis for the latter gets smaller and the corresponding higher states are determined less reliably.

For our main spectrum calculation we work with $N = 24$ operators in the 0^{++} channel, i.e. $\phi_k \in R, L, C, P, P_d, T$, each considered for at least two blocking levels. In the 2^{++} channel we choose $N = 23$ and $\phi_k \in R, L, C, P, T$. In the symmetric phase this typically enables us to obtain mass estimates for the first 10–12 states in each of these channels.

For spin-1 particles, we construct a 4×4 matrix correlator from the operator of type V considered at four blocking levels. Thereby we can extract masses for the first two or three states only. In the computation of separate correlations of the Polyakov loop operator itself, we also compute a 4×4 matrix correlator using different blocking levels.

---

[2]Note that on a finite volume, those states have a discrete spectrum.

For a more detailed discussion of the variational method based on matrix correlators, along with numerical investigations to test its efficiency, we refer to our previous work [4].

2.4 Simulation and analysis details

The Monte Carlo simulation of the lattice action in eq. (1) is performed using the same algorithms as in our previous work. The bare parameters β_G, β_H and β_R are fixed by applying the constraints $\lambda_3/g_3^2 = 0.0239$ and $\lambda_3/g_3^2 = 0.2743$, respectively, and using the same procedure as in section 3 of ref. [4]. For the update of gauge variables we use a combination of the standard heatbath and over-relaxation algorithms for SU(2) [21, 22]. The scalar degrees of freedom are updated using the algorithm described in [23]. In general, the applicability of this algorithm is restricted to cases where the self-coupling β_R is not too large, as otherwise the acceptance rate decreases substantially. In our simulation, however, we did not observe any significant drop in the acceptance rate, even at our larger value of β_R. Thus the algorithm may be applied safely in the region of the parameter space explored in this paper.

As before, we define a "compound" sweep to consist of a combination of one heatbath and several over-relaxation updates of the gauge and scalar fields. In the Higgs and confinement regions of the phase diagram at both small and large scalar coupling we typically gathered about 12000 compound sweeps for our main spectrum calculation. In the crossover region we also monitored the spectrum at several, closely spaced values of β_H, for which about 5000 compound sweeps were accumulated each. Thus, the statistics in our present study is much lower than in our previous work. At first sight this may seem surprising, since we now seek to obtain a more detailed structure of the mass spectrum. However, we wish to remark that our basis of operators is much larger than in [4], so that a loss in statistics is compensated for by using the information from a greater number of correlators in a particular channel. In addition, the diagonalisation procedure requires a large basis of operators in order to yield reliable results for the excitation spectrum.

Our standard lattice sizes in this study are 36^3 and 24^3, which, on the basis of our previous study, do not lead to significant finite-size effects in the 0^{++} and 1^{--} channels. In order to study finite-volume effects in more detail, especially in the 2^{++} channel, we have also simulated lattices of size $16^2 \cdot 24$.

Our mass estimates are extracted from two-parameter, correlated, single-exponential fits over a finite interval $[t_1, t_2]$ to correlation functions of eigenstates Φ_i (c.f. subsection 3.4 in ref. [4]). We have checked explicitly that the alternative fitting formula moti-

vated in [24], where an additional constant is considered, does not produce an appreciable difference in our mass estimates.

In cases where the effective masses calculated from the correlation function did not show a plateau long enough to perform a correlated fit, we used effective masses for our best estimates. This was also our preferred method for the scan of the crossover region, where we were more interested in qualitative features rather than very precise mass estimates. Results which were obtained from effective masses, or from eigenstates whose individual overlaps a_{ik} were small throughout, are marked by an asterisk in our data tables in sections 3 and 4.

Statistical errors are estimated using a jackknife procedure for which the individual measurements have been accumulated in bins of 500 sweeps. For some of our most precise results we also quote a systematic error, which was obtained by quoting the difference between our best estimate and the result from an uncorrelated fit, and, in some cases, the result obtained using an alternative fitting interval.

3 Results at small scalar coupling

To explore small scalar coupling physics we fix $\lambda_3/g_3^2 = 0.0239$ as in ref. [4]. In the context of the electroweak phase transition this value corresponds to a tree-level, zero temperature Higgs mass of around $35\,\mathrm{GeV}$. For this value the system exhibits a strong first order transition upon variation of β_H and the Higgs and confinement properties on each side of the transition are very pronounced and easily distinguishable. In the symmetric phase we choose the point $\beta_H = 0.3438$ and in the Higgs phase $\beta_H = 0.3450$. The 0^{++} and 1^{--} channels of the mass spectrum at these parameter values have already been determined in our previous work [4]. Here we repeat this calculation with a larger basis of operators in order to obtain more details about the excitation spectrum. We do so at $\beta_G = 9$, where we know from our previous study that we are already close to the continuum limit of the theory.

3.1 Mass eigenstates in the Higgs and confinement regions

The lowest states of the mass spectrum at the two points investigated are shown in Fig. 1 (a). In the confinement region one observes the now familiar, dense spectrum of states for the three spin channels. As an illustration of the contributions of different types of basic operators to the mass eigenstates, we plot the coefficients a_{ik} (c.f. eq. (10))
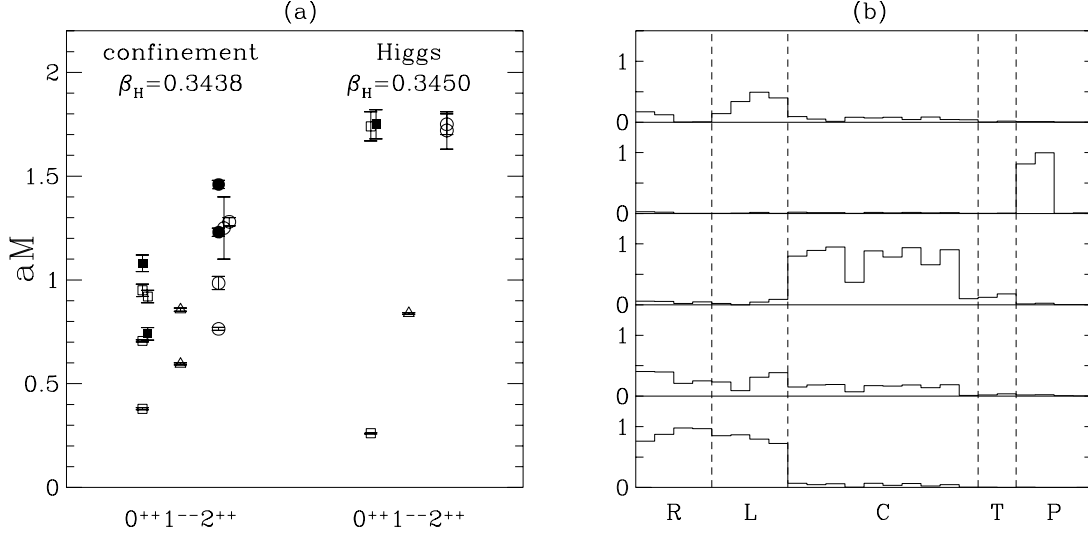
9

Figure 1: *(a) The lowest states of the spectrum in the confinement (left) and Higgs (right) region at small scalar coupling, $\beta_G = 9$. Full symbols indicate states that receive predominantly contributions from C-type operators. (b) The coefficients a_{ik} of the 24 operators used in the simulation for the five lowest 0^{++} eigenstates in the confinement phase.*

in Fig. 1 (b) for the lowest five eigenstates in the 0^{++} channel in the confining phase.

Our main results in the Higgs phase are listed in Table 1. Here, the only low-lying states are the familiar Higgs and W-boson states, which are also well described by perturbation theory. Note in particular that the lowest mass in the 2^{++} channel is rather large and consistent with that of a $W\,W$-scattering state – as are the excited states in the 0^{++} channel. In particular, consider one of the first excited states in the 0^{++} channel. This state has almost exclusively contributions from C-type operators, i.e. it consists mainly of gauge degrees of freedom. This suggests interpreting it as a $W\,W$-scattering state, and Table 1 shows that the mass of this state is indeed compatible with twice the W-mass. This result is also expected from perturbation theory, where the term with the slowest exponential fall-off corresponds to a two-W exchange diagram. It is natural to ask at this point why we do not see a two-Higgs state as the first excitation, since such a state is lighter than the two-W state. The reason is that our operators appear to have practically no projection on such a state. In order to see a two-Higgs state it would be necessary to study the correlations of an operator which by construction couples to such a state in leading order, for instance $(R(\vec{p}=0) - \langle R \rangle)^2$. This, however, is beyond the scope of this work.

No.	$16^2 \cdot 24$ aM	24^3 aM	J^{PC}
Φ_1	$0.2666(17) \, ^{+\,0}_{-27}$	$0.2613(28)$	0^{++}
Φ_2	$1.65(6)$	$1.74(7)^*$	0^{++}
Φ_3	$1.81(8)$	$1.75(7)^*$	0^{++}
Φ_1	$0.837(3) \, ^{+0}_{-4}$	$0.839(4)$	1^{--}
Φ_1		$1.75(5)^*$	2^{++}
Φ_2		$1.72(9)^*$	2^{++}

Table 1: *Results for all three spin channels in the Higgs region at $\beta_H = 0.3450$. The second error in some results is an estimate of systematic errors as described in subsect. 2.4.*

Our main results in the symmetric phase are listed in Tables 2–4. With our larger basis of operators we are able to identify a large number of states (e.g. up to 16 states in the 0^{++} channel), and quite a number of them receive their dominant contributions from Polyakov-loop or torelon-pair operators. Note in particular the change in the operator content in the ground state of the 2^{++} channel as the lattice size is increased. This will be discussed in more detail in connection with finite-size effects in the next subsection. Our results for the lowest masses are in agreement with our earlier study (c.f. Tables 2 and 3 in [4]), although we now obtain a slightly lower value for the mass of the W-boson.

The physical states consist of a dense spectrum of bound states. The second excited state in the 0^{++}-channel is a pure gauge excitation which, in this phase, cannot be perturbatively related to a two-W state. Instead it was suggested in [4] to interpret it as a W-ball in analogy to the glueballs of pure gauge theory. This interpretation is based on the observation that the state is composed predominantly from gauge degrees of freedom and that its mass nearly equals that of the lightest scalar glueball in the pure SU(2) gauge theory at this value of β_G. As Table 3 shows, there is a corresponding state in the 2^{++} channel. We also find higher excitations of these lowest W-ball states for both quantum numbers.

In Table 5 we compare some properties of the Polyakov loop operator in the Higgs and confinement regions. As explained in subsection 2.2, the Polyakov loop has a large expectation value in the Higgs phase, indicating the absence of confinement. Similar to the correlator of C-type operators, the perturbative expansion of the Polyakov loop correlator for weak coupling is dominated by a two-W exchange diagram, and indeed we find its exponential fall-off to be compatible with twice the W-mass. These findings are

$L^2 \cdot T = 36^3,$			$\beta_H = 0.3438$		
No.	$aM[0^{++}]$	Ops.	No.	$aM[0^{++}]$	Ops.
Φ_1	$0.379(5)\ {}^{+0}_{-7}$	R, L	Φ_7	$1.08(4)\ {}^{+2}_{-0}$	C
Φ_2	$0.706(5)\ {}^{+0}_{-5}$	R, L	Φ_8	$1.35(2)$	C
Φ_3	$0.74(3)^*$	C	Φ_9	$1.27(8)$	P
Φ_4	$0.84(2)$	P	Φ_{10}	$1.47(3)\ {}^{+0}_{-2}$	P
Φ_5	$0.95(3)$	L	Φ_{11}	$1.50(4)$	C
Φ_6	$0.92(3)\ {}^{+2}_{-0}$	R	Φ_{12}	$1.56(4)$	C
$L^2 \cdot T = 24^3,$			$\beta_H = 0.3438$		
No.	$aM[0^{++}]$	Ops.	No.	$aM[0^{++}]$	Ops.
Φ_1	$0.382(3)$	R	Φ_9	$1.10(2)$	P
Φ_2	$0.577(8)$	P	Φ_{10}	$1.27(2)^*$	C, T
Φ_3	$0.690(14)$	R	Φ_{11}	$1.25(3)^*$	L
Φ_4	$0.756(7)\ {}^{+6}_{-0}$	C	Φ_{12}	$1.44(3)\ {}^{+0}_{-2}$	T
Φ_5	$1.02(2)$	C	Φ_{13}	$1.51(4)$	C
Φ_6	$0.95(6)^*$	P_d	Φ_{14}	$1.33(3)$	L
Φ_7	$1.03(2)$	L, C	Φ_{15}	$1.50(4)$	T
Φ_8	$0.99(2)$	P_d	Φ_{16}	$1.55(6)$	P_d
$L^2 \cdot T = 16^2 \cdot 24,$			$\beta_H = 0.3438$		
No.	$aM[0^{++}]$	Ops.	No.	$aM[0^{++}]$	Ops.
Φ_1	$0.315(9)\ {}^{+13}_{-\ 0}$	P	Φ_8	$0.87(5)$	L
Φ_2	$0.40(2)$	S	Φ_9	$1.08(8)^*$	C
Φ_3	$0.64(2)$	P_d	Φ_{10}	$1.45(3)^*$	C
Φ_4	$0.723(8)\ {}^{+0}_{-8}$	C	Φ_{11}	$1.20(15)^*$	P_d
Φ_5	$0.78(7)^*$	S	Φ_{12}	$1.49(3)$	C
Φ_6	$0.96(5)$	T	Φ_{13}	$1.28(9)$	L
Φ_7	$0.96(4)$	P			

Table 2: *Mass spectrum and dominant contributions from the operator basis in the 0^{++} channel at small scalar self-coupling in the symmetric phase.*

$L^2 \cdot T = 36^3,$			$\beta_H = 0.3438$		
No.	$aM[2^{++}]$	Ops.	No.	$aM[2^{++}]$	Ops.
Φ_1	0.764(7)	L	Φ_6	1.46(2)	C
Φ_2	0.888(8) $^{+5}_{-0}$	P	Φ_7	1.25(15)*	P
Φ_3	0.985(32)	R, L	Φ_8	1.2(2)*	P
Φ_4	1.23(2)	C	Φ_9	1.6(1)	C
Φ_5	1.28(2)	R			
$L^2 \cdot T = 24^3,$			$\beta_H = 0.3438$		
No.	$aM[2^{++}]$	Ops.	No.	$aM[2^{++}]$	Ops.
Φ_1	0.570(5) $^{+0}_{-4}$	P	Φ_6	1.29(2)(2)	T
Φ_2	0.791(9)	L	Φ_7	1.31(3) $^{+3}_{-0}$	R, L, C
Φ_3	1.01(2)	R	Φ_8	1.47*	C
Φ_4	1.09(2)	P	Φ_9	1.49(4)	R
Φ_5	1.1(1)*	C			
$L^2 \cdot T = 16^2 \cdot 24,$			$\beta_H = 0.3438$		
No.	$aM[2^{++}]$	Ops.	No.	$aM[2^{++}]$	Ops.
Φ_1	0.361(12) $^{+6}_{-0}$	P	Φ_6	1.5(1)*	C
Φ_2	0.843(27)	T	Φ_7	1.4(1)*	L, R
Φ_3	0.86(2)	L	Φ_8	1.55(4)	C, T
Φ_4	0.98(4) $^{+0}_{-1}$	P	Φ_9	1.6(2)*	L
Φ_5	1.18(5) $^{+3}_{-0}$	C	Φ_{10}	1.79(7)	C

Table 3: *Mass spectrum and dominant contributions from the operator basis in the 2^{++} channel at small scalar self-coupling in the symmetric phase.*

$\beta_H = 0.3438$			
	$L^2 \cdot T = 36^3$	$L^2 \cdot T = 24^3$	$L^2 \cdot T = 16^2 \cdot 24$
No.	$aM[1^{--}]$	$aM[1^{--}]$	$aM[1^{--}]$
Φ_1	0.595(5) $^{+0}_{-6}$	0.582(14)	0.585(15) $^{+17}_{-0}$
Φ_2	0.857(8) $^{+12}_{-0}$	0.863(9) $^{+0}_{-7}$	0.99(2)*
Φ_3	0.98(8)*	1.068(18) $^{+0}_{-14}$	1.15(4)

Table 4: *Mass spectrum in the 1^{--} channel at small scalar self-coupling in the symmetric phase.*

$L^2 \cdot T$	Confinement $\beta_H = 0.3438$			Higgs $\beta_H = 0.3450$	
	36^3	24^3	$16^2 \cdot 24$	$16^2 \cdot 24$	24^3
$\langle P_1^{(L)} \rangle$	0.001(10)	0.001(10)	0.14(2)	6.535(6)	6.724(5)
aM_P	$0.879(6)\,^{+0}_{-2}$	0.570(4)	0.366(3)	1.67(4)	$1.54(4)^*$
$aM[1^{--}]$	$0.595(5)\,^{+0}_{-6}$	0.582(14)	$0.585(15)\,^{+17}_{-0}$	0.839(4)	$0.837(3)\,^{+0}_{-4}$
$a\sqrt{\sigma_\infty}$	$0.1575(5)\,^{+0}_{-2}$	$0.1570(6)\,^{+0}_{-2}$	0.1579(5)	–	–

Table 5: *Properties of the Polyakov loop operator in the confinement and Higgs region for $\beta_G = 9$. $\langle P_1^{(L)} \rangle$ here refers to the unsmeared operator.*

supported by the observation that the mass extracted from the correlation of Polyakov loops is roughly independent of the spatial lattice size L, in sharp contrast to situations where confinement is observed.

In the symmetric phase, on the other hand, we find that the expectation value of the Polyakov loop is consistent with zero, indicating confinement at small distances. Here, ordinary weak coupling expansions fail, and the exponential fall-off of the correlation of Polyakov loops is incompatible with twice the W-mass, c.f. Table 5. Instead, one interprets it as the mass of a loop of chromoelectric flux, aM_P, which can be related to the string tension σ_L

$$\sum_{\vec{x}} \left\langle P_j^{(L)}(x) P_j^{(L)\dagger}(0) \right\rangle \simeq e^{-aM_P(L)t}, \quad aM_P(L) = a^2 \sigma_L L. \tag{11}$$

Here L is the spatial length of the lattice and hence of the flux loop. An estimate for the string tension in infinite volume is then provided by the relation [25]

$$a^2 \sigma_\infty = a^2 \sigma_L + \frac{\pi}{6L^2}. \tag{12}$$

We add that our numerical values for the string tension $a\sqrt{\sigma_\infty}$ shown in Table 5 are only around 3% smaller than in the pure gauge theory [27].

3.2   Finite-volume effects and toroidal operators

In this subsection we consider the issue of finite-size effects in more detail. In particular, we want to clarify the rôle of toroidal (or winding) operators, i.e. operators constructed out of Polyakov loops, for finite-volume studies in QCD-like situations. This is of particular relevance in the symmetric phase of our model, where we have reported strong

finite-size effects in the ground state of the 0^{++} channel[4]. Although we include this discussion in the section on small scalar coupling, our findings are relevant at large coupling as well.

Toroidal operators, such as the Polyakov loop, project mainly onto states encircling the periodic boundary conditions, sometimes called "torelons"[20] (see also eq. (11)). These torelon states can interfere with the mass spectrum of the theory in infinite volume if

$$a^2 \sigma_L L \lesssim aM, \tag{13}$$

where M is the mass of an eigenstate of the Hamiltonian. It should be stressed at this point that torelon states exist in the continuum limit for finite box size and periodic boundary conditions. Thus they are not lattice artefacts, i.e. artefacts arising from the discretisation of the theory.

As explained in subsection 2.2, we use blocked operators in the 0^{++} and 2^{++} channels, which, due to the iterative nature of the blocking procedure, may accidentally contain contributions which wind around the lattice and can thus have a sizeable projection onto torelon states. If relation (13) applies this can then lead to a possible misidentification of the ground state and/or higher excitations of the Hamiltonian. This scenario does not apply in the 1^{--} channel, where it is impossible to construct a torelon operator with the same quantum numbers. Furthermore, the overlap between single torelons and W-ball operators will be strongly suppressed as long as we have approximate confinement and the associated approximate Z_2 symmetry, under which torelon and W-ball operators transform differently. However, torelon-antitorelon pairs can have a big influence on the spectrum of W-balls and are therefore included in our study.

As an illustration of the issue, consider Fig. 1 (b) and Table 2. The analysis of the operator content shows Φ_4 to have almost exclusively P-content. The mass associated with it is a flux loop mass appropriate to extract the string tension, but it is not part of the spectrum of the Hamiltonian in infinite volume and has to be removed. An example how these toroidal states mix with the physical ones and have to be carefully disentangled is given for the case of the 2^{++} spectrum in Fig. 2 and Table 3. On the smaller lattice, Fig. 2 (a), the lowest state is a mixture of R/L and P-type operators, with a slight dominance by P. Quoting the corresponding mass as a physical state close to its infinite-volume limit would be erroneous, as is elucidated by considering the same operators on a larger volume. The masses arising from winding operators have become heavier (see eq. (13)), while the non-winding operators produce mass values which hardly change under variation of the volume, and are thus already close to infinite-volume physics. Com-
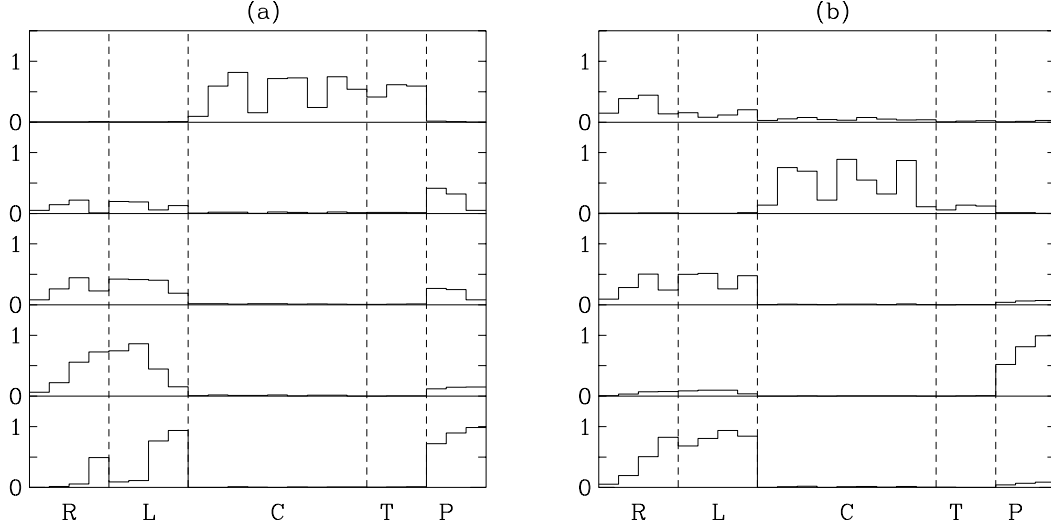
Figure 2: *The coefficients a_{ik} of the 23 operators used in the simulation for the five lowest 2^{++} eigenstates, (a) $L = 24$, (b) $L = 36$.*

bining the information about the overlaps of individual operators with their behaviour as the spatial lattice size is increased makes the identification of the masses which are part of the spectrum in the infinite-volume limit unambiguous.

As a result, some of the conclusions concerning the finite-volume behaviour in ref. [4] have to be revised. First, the large finite-volume effects in the 0^{++} channel clearly arise from toroidal operators, as the relation (13) certainly holds in the 0^{++} channel for the smallest lattices considered in our previous work. Second, our new findings remove the anomalous behaviour of the first excited state. This can be understood since the ordering of the excitation spectrum changes with increasing lattice size, as toroidal operators will produce more and more massive states.

3.3   The physical spectrum

After removing finite size effects introduced by considering toroidal operators, we are ready to present our final mass estimates for the spectrum in Table 6. In addition to the mass spectrum extracted from our simulations of the SU(2) Higgs model, the glueball spectrum of the pure SU(2) gauge theory is also given [26, 27].

For all cases considered we find that the W-ball masses deviate from those of the glueballs at the percent level at most. Thus, the glueball spectrum of the pure gauge

0++ channel			2++ channel		
Gauge-Higgs		Pure Gauge	Gauge-Higgs		Pure Gauge
Scalar	W-ball	W-ball	Scalar	W-ball	W-ball
$0.379(5)\,^{+0}_{-7}$			$0.764(7)$		
$0.706(5)\,^{+0}_{-5}$			$0.99(3)$		
	$0.74(3)^*$	$0.767(6)$		$1.23(2)$	$1.26(2)$
$0.95(3)$			$1.28(2)$		
$0.92(3)\,^{+2}_{-0}$			$1.25(15)^*$		
	$1.08(4)\,^{+2}_{-0}$	$1.08(2)$		$1.46(2)$	$1.50(5)$
	$1.35(2)$	$1.27(2)$		$1.64(4)^*$	$1.77(6)$
			$1.67(6)$		

Table 6: *Final mass estimates using the data obtained on 36^3 at $\beta_G = 9$, $\beta_H = 0.3438$ in the symmetric phase at small scalar self-coupling. Our data for the W-ball are compared to results obtained in the pure gauge theory.*

theory is almost identically repeated in the scalar-gauge theory and appears to be entirely insensitive to the presence of the scalar fields. In addition, and apparently disjoint from this part of the spectrum, there are bound states of scalars which also have some gauge content. Combining this observation with the practically identical value of the string tension, we confirm our earlier conclusion [4] that the pure gauge sector of the theory decouples almost completely from the Higgs sector at this point in the symmetric phase.

4 Results at large scalar coupling

It is now interesting to study whether a significant increase of the scalar self coupling destroys the decoupling of the pure gauge sector observed for small coupling. For this purpose we fix the ratio of scalar and gauge couplings to be about ten times larger than previously, $\lambda_3/g_3^2 = 0.2743$. At this parameter value the first order phase transition between the Higgs and the confinement regions upon variation of β_H has disappeared and turned into a smooth crossover [8, 2]. One would expect that the absence of a phase transition weakens the specific Higgs and confinement properties on the respective "sides" of the crossover. For the simulations the points $\beta_H = 0.35262$ and $\beta_H = 0.35542$ are chosen to represent the confinement and Higgs sides of the phase diagram, respectively.

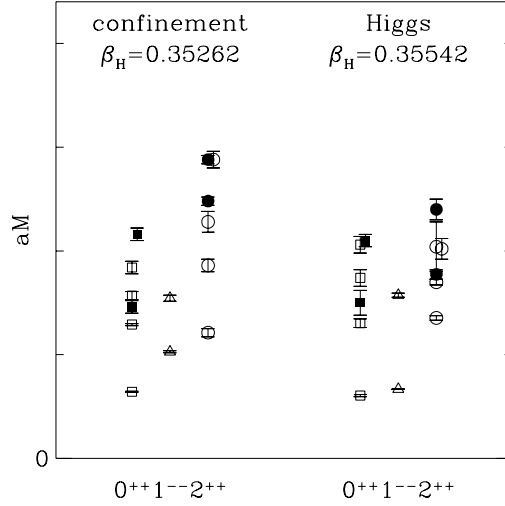The lowest states of the mass spectrum are shown in Fig. 3. Higher excitations as

Figure 3: *The lowest states of the spectrum in the confinement (left) and Higgs (right) region. Full symbols indicate states that receive predominantly contributions from C-type operators.*

well as the composition of all states can be found in Tables 7-11. The spectrum in the confinement region looks qualitatively the same as in the small scalar coupling case. In particular, we observe the same occurrence of W-ball states in the 0^{++} and 2^{++} channels as well as their non-mixing with the bound states of scalars as for small scalar coupling, c.f. Tables 7, 8. By comparing the numerical values of the W-ball masses at small and large scalar coupling, one finds that all W-ball masses agree quantitatively, i.e. are statistically compatible, with those at small scalar coupling. Thus the previously stated decoupling of the pure gauge sector from the Higgs part of the theory extends over an order of magnitude increase in the ratio of scalar coupling to gauge coupling!

On the Higgs side of the crossover, a dramatic change in the nature of the spectrum has taken place. The specific "Higgs-like" feature of having only the Higgs and W-particle as low lying states with a large gap to higher excitations has entirely disappeared. Instead, we now have a dense spectrum of states on the Higgs side as well, which differs only quantitatively from the one on the confinement side. Note that the value for the scalar coupling considered here is so large that perturbation theory is not reliable anymore [28].

Let us now look at the expectation value of the Polyakov loop. The points where we analysed the mass spectrum correspond to the endpoints in Fig. 4, where the expectation value of the Polyakov loop is shown. Note that now there is a small but non-zero, measur-

$L^2 \cdot T = 36^3,$		$\beta_H = 0.3526$			
No.	$aM[0^{++}]$	Ops.	No.	$aM[0^{++}]$	Ops.
Φ_1	$0.321(3)$	R,L	Φ_8	$1.06(6)^*$	S
Φ_2	$0.645(5)\,{}^{+0}_{-3}$	R,L	Φ_9	$1.33(3)(1)$	C
Φ_3	$0.73(3)$	C	Φ_{10}	$1.21(9)^*$	L
Φ_4	$0.850(7)\,{}^{+3}_{-0}$	P	Φ_{11}	$1.40(3)^*$	P
Φ_5	$0.785(19)$	L	Φ_{12}	$1.56(4)^*$	C
Φ_6	$0.92(3)\,{}^{+0}_{-2}$	R,L	Φ_{13}	$1.60(4)$	C
Φ_7	$1.08(3)\,{}^{+0}_{-2}$	C	Φ_{14}	$1.74(5)$	T
$L^2 \cdot T = 24^3,$		$\beta_H = 0.3526$			
No.	$aM[0^{++}]$	Ops.	No.	$aM[0^{++}]$	Ops.
Φ_1	$0.324(4)$	L	Φ_9	$1.10(3)$	
Φ_2	$0.543(9)$	P	Φ_{10}	$1.17(3)$	C,T
Φ_3	$0.661(7)$	R,L,P	Φ_{11}	$1.18(3)$	C,T
Φ_4	$0.737(12)$	C	Φ_{12}	$1.42(3)^*$	T
Φ_5	$0.752(23)\,{}^{+\,0}_{-26}$	L	Φ_{13}	$1.3(2)^*$	L
Φ_6	$0.968(12)$	R,L	Φ_{14}	$1.53(3)$	C,T
Φ_7	$0.98(3)$	C,P_d	Φ_{15}	$1.53(4)$	C,T
Φ_8	$1.03(2)$	C,P_d			

Table 7: *Mass spectrum and dominant contributions from the operator basis in the 0^{++} channel at large scalar self-coupling in the symmetric phase.*

$L^2 \cdot T = 36^3,$			$\beta_H = 0.3526$		
No.	$aM[2^{++}]$	Ops.	No.	$aM[2^{++}]$	Ops.
Φ_1	$0.606(20)\ ^{+11}_{-\ 0}$	R,L	Φ_7	$1.45(3)$	P
Φ_2	$0.859(17)\ ^{+\ 0}_{-15}$	P	Φ_8	$1.44(4)^*$	R
Φ_3	$0.93(3)^*$	R,L	Φ_9	$1.62(4)$	C
Φ_4	$1.24(2)^*$	C	Φ_{10}	$1.2(2)^*$	L
Φ_5	$1.14(5)^*$	L	Φ_{11}	$1.6(1)^*$	C,T
Φ_6	$1.44(2)$	C	Φ_{12}	$1.81(4)$	C,T
$L^2 \cdot T = 24^3,$			$\beta_H = 0.3526$		
No.	$aM[2^{++}]$	Ops.	No.	$aM[2^{++}]$	Ops.
Φ_1	$0.568(5)\ ^{+3}_{-0}$	P	Φ_6	$1.29(2)\ ^{+0}_{-1}$	C,T
Φ_2	$0.734(23)$	L	Φ_7	$1.22(2)\ ^{+0}_{-2}$	L
Φ_3	$1.02(2)\ ^{+0}_{-1}$	R	Φ_8	$1.48(4)\ ^{+0}_{-2}$	C
Φ_4	$1.12(2)$	P	Φ_9	$1.40(15)^*$	R
Φ_5	$1.22(3)$	C,T	Φ_{10}	$1.65(5)$	R

Table 8: *Mass spectrum and dominant contributions from the operator basis in the 2^{++} channel at large scalar self-coupling in the symmetric phase.*

able value for the expectation value of the Polyakov loop on the confinement side. This is a first indication that confinement will eventually be screened at very large distances. On the other hand, at the Higgs end we measure a large expectation value, just as in the case of small scalar coupling. Comparing the two sides in Fig. 3 one might be inclined to conclude that the similarity of the spectra indicates an extension of the confining physics over to the Higgs side of the crossover, which seems not unreasonable given the absence of a real transition. However, from the large difference in the expectation value for the Polyakov loop we are led to conclude that the dynamics responsible for the dense spectrum on the Higgs side must be very different from that on the confinement side. In particular, no flux loops exist on this side of the crossover. This may be an indication that what we see in this region of the phase diagram is a strong scalar coupling Higgs regime. More numerical and analytic evidence is required, though, to verify this interpretation.

Our final mass estimates for the physical states in the confinement phase, with the toroidal operators removed as in the previous section, are given in Table 12.

$L^2 \cdot T = 36^3$,		$\beta_H = 0.3554$			
No.	$aM[0^{++}]$	Ops.	No.	$aM[0^{++}]$	Ops.
Φ_1	$0.303(5)\ ^{+4}_{-1}$	R, L	Φ_9	$1.02(4)$	(P, T, P_d)
Φ_2	$0.652(21)\ ^{+\ 0}_{-15}$	L, C, P, T, P_d	Φ_{10}	$1.33(2)$	C
Φ_3	$0.80(4)$	P, T, P_d	Φ_{11}	$1.32(2)$	C
Φ_4	$0.75(6)^*$	C	Φ_{12}	$1.39(4)\ ^{+0}_{-2}$	P_d
Φ_5	$0.75(5)^*$	$C, (P)$	Φ_{13}	$1.41(3)$	C, T
Φ_6	$1.05(3)\ ^{+0}_{-1}$	C	Φ_{14}	$1.51(3)\ ^{+0}_{-1}$	C, T
Φ_7	$0.87(4)\ ^{+0*}_{-1}$		Φ_{15}	$1.53(4)$	C, T
Φ_8	$1.03(4)^*$				
$L^2 \cdot T = 24^3$,		$\beta_H = 0.3554$			
No.	$aM[0^{++}]$	Ops.	No.	$aM[0^{++}]$	Ops.
Φ_1	$0.317(3)\ ^{+0}_{-6}$	L	Φ_7	$1.05(5)^*$	C
Φ_2	$0.642(14)\ ^{+\ 0}_{-16}$	L, P	Φ_8	$1.20(2)$	C
Φ_3	$0.704(24)$	P, T	Φ_9	$1.21(3)$	C, P, T
Φ_4	$0.82(5)$	L	Φ_{10}	$1.30(3)$	$T, (C)$
Φ_5	$0.87(2)^*$	C	Φ_{11}	$1.37(3)$	P, T
Φ_6	$0.9(1)^*$		Φ_{12}	$1.37(4)$	C, T

Table 9: *Mass spectrum and dominant contributions from the operator basis in the 0^{++} channel at large scalar self-coupling in the broken phase. Labels in brackets indicate that the contribution from the corresponding operator are small but significant.*

$L^2 \cdot T = 36^3,$		$\beta_H = 0.3554$			
No.	$aM[2^{++}]$	Ops.	No.	$aM[2^{++}]$	Ops.
Φ_1	0.677(11)	L	Φ_7	$1.2(1)^*$	L
Φ_2	0.849(13)	R,L,P,T	Φ_8	1.43(4)	C
Φ_3	0.887(22)	(C)	Φ_9	1.44(2)	C
Φ_4	1.02(12)	(R,L)	Φ_{10}	1.57(4)	L
Φ_5	$1.01(5)\,{}^{+0}_{-3}$	(R)	Φ_{11}	$1.51(3)\,{}^{+1}_{-0}$	T
Φ_6	$1.20(5)\,{}^{+0}_{-2}$	C			
$L^2 \cdot T = 24^3,$		$\beta_H = 0.3554$			
No.	$aM[0^{++}]$	Ops.	No.	$aM[0^{++}]$	Ops.
Φ_1	$0.639(8)\,{}^{+\,0}_{-22}$	L	Φ_6	1.10(7)	C
Φ_2	$0.84(3)^*$	R,L	Φ_7	1.11(8)	T
Φ_3	0.87(4)	C	Φ_8	1.34(3)	C
Φ_4	$0.95(10)^*$	R	Φ_9	$1.34(2)\,{}^{+0}_{-2}$	C
Φ_5	1.21(3)	L	Φ_{10}	1.46(6)	

Table 10: *Mass spectrum and dominant contributions from the operator basis in the 2^{++} channel at large scalar self-coupling in the broken phase. Labels in brackets indicate that the contribution from the corresponding operator are small but significant.*

	$\beta_H = 0.3526$		$\beta_H = 0.3554$	
	$L^2 \cdot T = 36^3$	$L^2 \cdot T = 24^3$	$L^2 \cdot T = 36^3$	$L^2 \cdot T = 24^3$
No.	$aM[1^{--}]$	$aM[1^{--}]$	$aM[1^{--}]$	$aM[1^{--}]$
Φ_1	0.514(5)	$0.482(15)\,{}^{+41}_{-10}$	$0.3341(12)\,{}^{+\,0}_{-14}$	0.3313(27)
Φ_2	$0.772(15)\,{}^{+6}_{-0}$	0.80(2)	0.787(10)	0.822(17)
Φ_3	$0.94(4)\,{}^{+1}_{-0}$	0.94(5)	1.040(16)	$0.99(8)^*$

Table 11: *Mass spectrum in the 1^{--} channel at large scalar self-coupling in the symmetric and broken phases.*

0^{++} channel			2^{++} channel		
Gauge-Higgs		Pure Gauge	Gauge-Higgs		Pure Gauge
Scalar	W-ball	W-ball	Scalar	W-ball	W-ball
0.321(3)			0.61(2) $^{+1}_{-0}$		
0.645(5) $^{+0}_{-3}$			0.93(3)*		
	0.73(3)	0.767(6)		1.24(2)*	1.26(2)
0.79(2)			1.14(5)*		
0.92(3) $^{+0}_{-2}$			1.44(4)*		
	1.08(3) $^{+0}_{-2}$	1.08(2)		1.44(2)	1.50(5)
	1.33(3)	1.27(2)		1.62(4)	1.77(6)

Table 12: *Final mass estimates using the data obtained on 36^3 at $\beta_G = 9$, $\beta_H = 0.3526$ in the symmetric phase at large scalar self-coupling. Our data for the W-ball are compared to results obtained in the pure gauge theory.*

5 The crossover region

As we have seen in the last section, the mass spectra of the Higgs and confinement regions are rather similar at large scalar coupling, although the underlying dynamics must be quite different. Since there is no phase transition but only a smooth crossover "separating" the respective regions at large scalar coupling one can study how the spectra are continuously connected. Apart from mapping the spectra in the Higgs and confinement regions onto each other, this also offers the opportunity to follow the change in the dynamics as one moves from one regime into the other.

We start by considering the expectation values of the Polyakov loop and the length of the Higgs field, displayed in Fig. 4. In most simulations dealing with the phase transition R has been used as an "order parameter", as it jumps across a first order phase transition from small values in the confinement phase to large values in the Higgs phase. As Fig. 4 illustrates, this jump has entirely disappeared, the change in $\langle R \rangle$ is smooth and very slow, with its values differing by only $\sim 30\%$ at the end points studied in the last section. On the other hand, as mentioned in the previous section, the expectation value of the Polyakov line is quite different at both ends of the curve. Because it probes confining behaviour and the change in dynamics in this region of parameter space, the expectation value of the Polyakov loop is more sensitive to the changes between the regions and hence makes a better "order parameter". However, strictly speaking it has to remain non-zero on the confinement side as well, so the change is smooth and quantitative only,
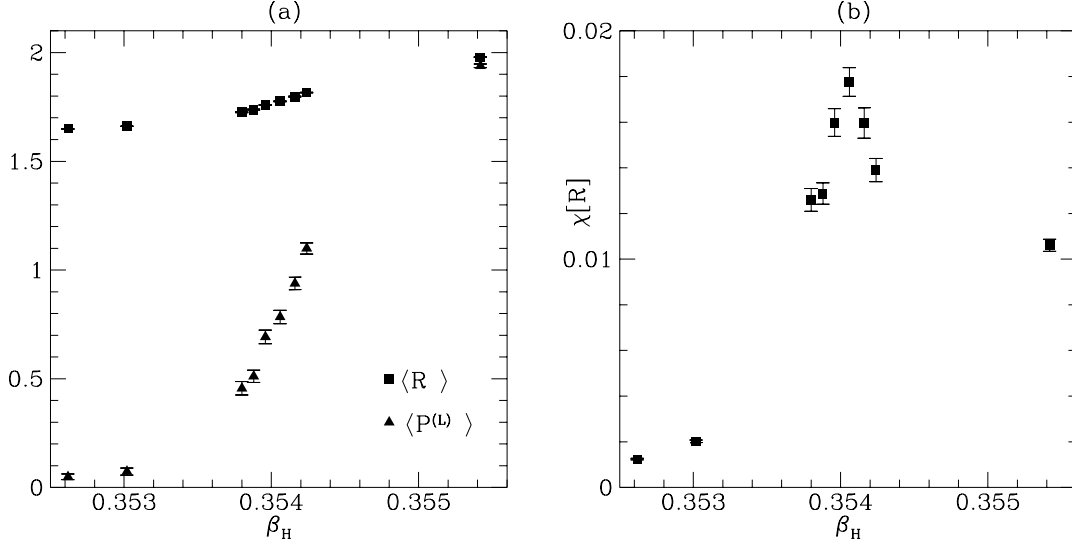
Figure 4: *(a) Vacuum expectation values for R and P. (b) Susceptibility of a smeared R-operator.*

as expected for a crossover.

Despite the smoothness of the crossover, it is possible to define a critical hopping parameter through the peak of the susceptibility of various quantities. We obtained the best signal for the susceptibility of a smeared version of our R-operator,

$$\chi = \langle R^2 \rangle - \langle R \rangle^2 \ . \tag{14}$$

In Fig. 4 (b) one easily identifies a pronounced peak in the suceptibility indicating large fluctuations in the operator under consideration. As in ref. [2] this peak serves to locate the critical value of the hopping parameter β_H^c at which the crossover takes place, and thus still represents a line "separating" the Higgs and confinement regions even in the absence of a phase transition. At $\beta_G = 9$ we estimate it to be $\beta_H^c = 0.35406(5)$.

The variation of the lowest states in the 0^{++} and 1^{--}-channels along the crossover is shown in Fig. 5. The mass of the lightest state of the theory, the 0^{++} ground state, shows a dip as the crossover is traversed. We have measured this mass on lattices of size $L = 24, 36$ and found no lowering of the mass with increasing lattice size. This means that essentially the infinite volume mass is reached and that the physical ground state mass definitely stays non-zero at the critical coupling. This identifies the transition unambiguously as a crossover [8, 2]. It is interesting to note that the mass of the third excited state, corresponding to the W-ball on the confinement side, does not change through
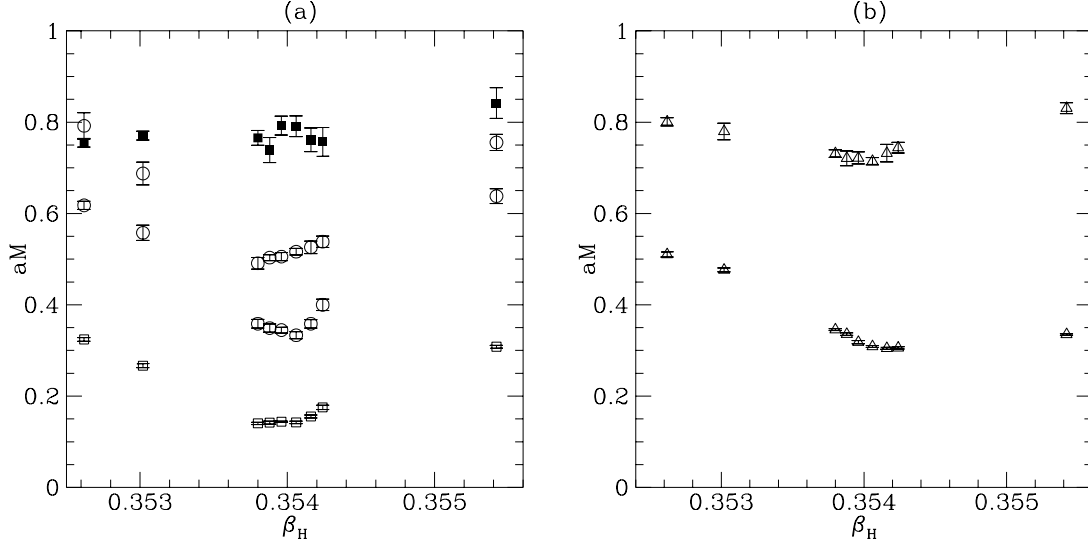
Figure 5: *Connecting the mass spectrum through the crossover. (a) The four lowest 0^{++} states. Empty squares denote the scalar gound state and full squares the W-ball. Circles correspond to mixed intermediate states. (b) The two lowest 1^{--} states.*

the crossover region until well into the Higgs region. This is yet another manifestation of its decoupling, this time it proves stable under variation of another scalar coupling parameter, the hopping parameter β_H.

In the 1^{--} channel we show only the lightest state and the first excitation, as our basis is smaller in this channel. The lowest state clearly becomes lighter as one changes from the confinement region to the Higgs region.

When the parameter β_H is varied through the crossover some states change their ordering in mass, so that we felt unable to assign distinct symbols to some of the states in Fig. 5 (a). In these cases the question arises how one identifies the individual states. A useful criterion is to look at the composition of the mass eigenstates in terms of the original operators used. As an example, we show the variation of the operator content of the 0^{++} ground state and W-ball through the crossover region in Fig. 6. The figure exhibits a remarkable phenomenon concerning the mixing of operators. As one moves from the confinement region towards the Higgs region, the scalar ground state picks up more contributions from purely "gluonic" operators. The mixing of scalar and gluonic operators is strongest in the middle of the crossover, at the critical coupling β_H^c. This is not unexpected given the fact that here the fluctuations are strongest. Although there is now a significant gauge contribution to the lowest state, it still remains clearly dominated
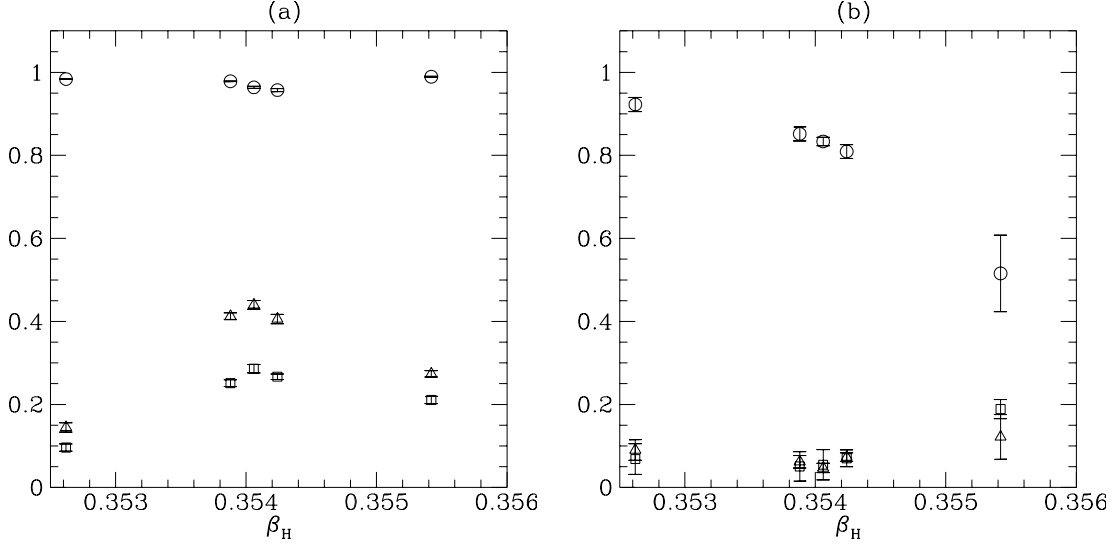
25

Figure 6: *Operator content through the crossover in the 0^{++}-channel. a) The ground state, b) The W-ball. Circles denote the maximal a_{ik} from R/L contributions, squares those from C and triangles represent the admixture of $P^{(L)}$.*

by scalar operators. Moving into the Higgs region the gauge contribution declines again and settles at some low value. Looking at the composition of the W-ball, however, we do not see the analogous feature happening. In contrast, the W-ball maintains its almost pure gauge composition throughout the crossover beyond the critical coupling, with equally low overlap with the Polyakov loop. Only as one moves clearly into the Higgs phase does the W-ball give up its purely gluonic nature, consistent with the decoupling observed form the behaviour of its mass.

Given the intrinsic interest of this decoupling phenomenon it is worth investigating it in more detail. To do so we take the lowest 13 states in the 0^{++} sector and display for each state the maximum overlap onto scalar (R or L) operators as well as the maximum overlap onto the gauge (C) operators. We do so separately for the confining and Higgs coupling values as well as for three values of β_H that correspond to traversing the crossover region from near the edge (on the confining side) to near the pseudo-critical value, β_H^c. The corresponding plots are shown on the left of Fig. 7. (Errors are not shown since they are small.) Those points shown as crosses correspond to states with substantial overlap onto flux loop operators. If the states had random scalar-gauge content, the points would be scattered over the whole plot. On the other hand, if there was a total scalar-gauge decoupling, then one or the other coordinate of each point would be zero. It is clear from Fig. 7 that the latter is close to being the case in the confining phase and that this
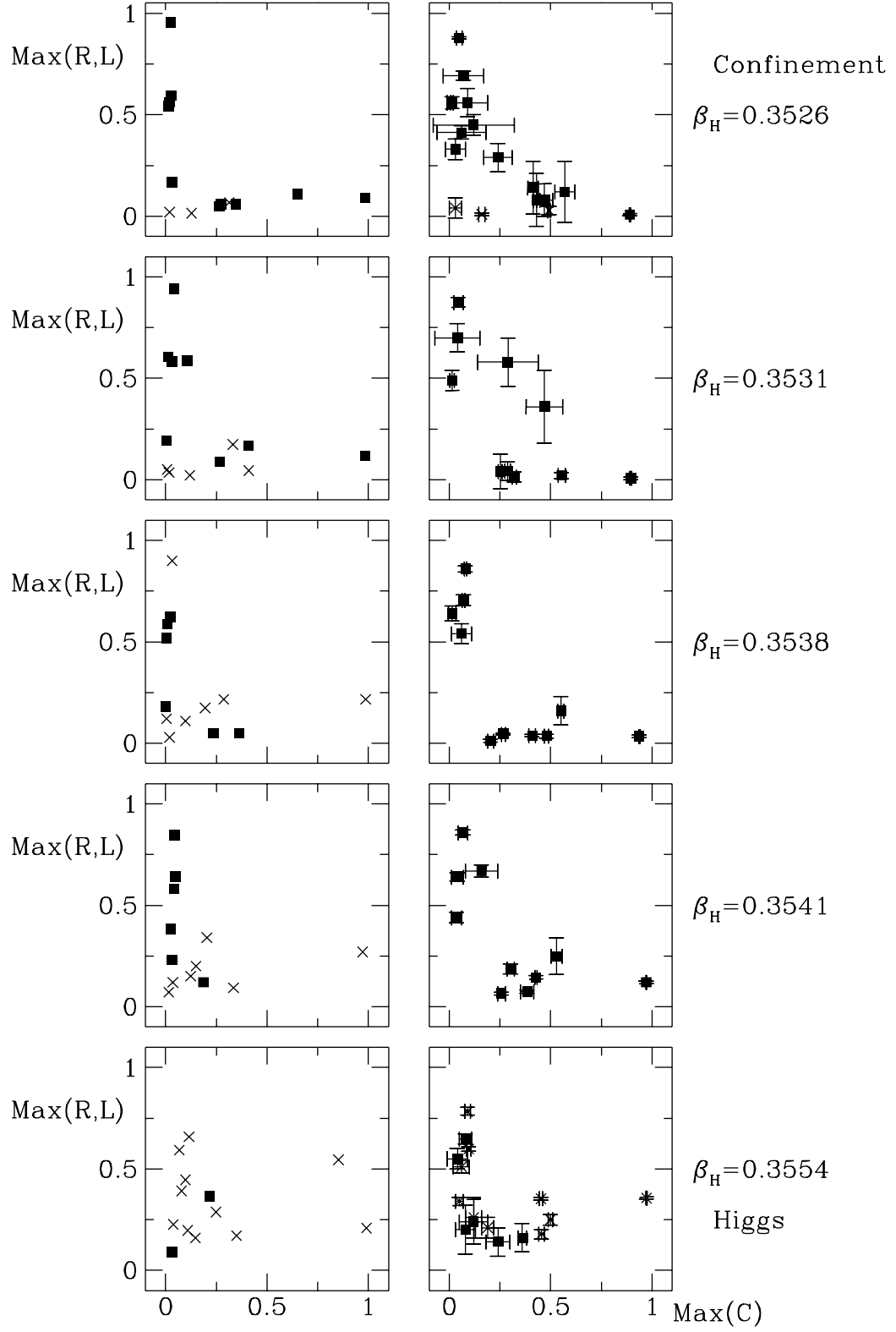
26

Figure 7: *Variation of the operator content of the 0^{++} (left) and 2^{++} (right) spectrum through the crossover as described in the text.*

persists, although more weakly, as we traverse the crossover region. In the Higgs phase, however, any decoupling effect is clearly much weaker. Note the increasing number of states with a substantial flux loop overlap, as we traverse the crossover towards the Higgs region. This is a manifestation of the increasing instability of the confining flux tube that we shall discuss in more detail below.

Also in Fig. 7, on the right, we show similar plots for the 2^{++}. In this case we show the errors because several of them are large. The reason for such large errors is that we have two almost degenerate states whose order is inverted in some measurements, relative to other measurements. That is to say, any point with large errros is definitely not an approximate state of the system and should hence be disregarded. If we do disregard those "states" then we see that we have a picture very similar to the one we obtained for the 0^{++}: a marked scalar-gauge decoupling in the confining region that only begins to weaken at the very centre of the crossover region. Indeed there seems to be some remnant of it even in the Higgs phase.

6   Flux-tube decay

When comparing the spectrum on the Higgs and confinement side of the first-order phase transition at small scalar coupling we discussed the different interpretations that the mass governing the exponential fall-off of the Polyakov line operator has: on the Higgs side it can be identified with the volume-independent mass of a two-W state while on the confinement side it rises linearly with the lattice size and represents a flux loop. These different behaviours represent the different dynamics in the two regimes. In this section we try to answer the question how the physics changes from the former interpretation to the latter. We know that the two regimes are analytically connected, and so are the mass eigenstates of the Higgs and confinement regimes. Hence, there must also be a smooth transition in the projection of the Polyakov line operator.

First, we note that we lose the signal for the mass aM_P as we move into the crossover region from either side. At the end-points in both regimes we do see plateaux in the effective mass, but they are lost when moving closer towards β_H^c. The situation is not improved by increasing the statistics. Second, let us recall that the Polyakov loop operator has an increasing projection onto the scalar ground state towards the middle of the crossover. These two observations may be given a physical interpretation. On the confinement side of the crossover we saw already a small non-vanishing expectation value for the Polyakov loop operator. Nevertheless, the mass extracted from the exponential

fall-off of its correlator still exhibits the linear dependence on the lattice size and hence represents a flux loop winding around the lattice, despite the fact that our model is not exactly confining, due to the presence of matter fields. As we move towards the critical point the Polyakov loop starts to develop an expectation value which signals the breakdown of linear confinement, so that flux loops no longer exist. The question then is, what happens to the flux loop as the parameters are changed? The increasing overlap of the Polyakov loop with the 0^{++} ground state suggests a natural explanation: As we move out of the confining region the flux loop becomes more and more unstable, as it is increasingly easy to pair-produce scalars that screen the flux. The 0^{++} ground state is one possible decay product, just based on quantum numbers. A stronger mixing between this state and the flux loop may thus indicate the increasing instability of the latter.

In order to elaborate on this point we consider the overlap of the Polyakov loop with all the 0^{++} eigenstates. If the suggested picture is true then all these states are possible decay products. Of course, there are other decay products as well, like pairs of 1^{--} particles etc. For a first qualitative test of our picture it is however sufficient to consider just the single particle states. Let us now treat the flux loop like a decaying resonance. As long as it is stable, its two-point correlation function has a pole at its mass. When the resonance becomes unstable the pole is shifted away from the real axis. The real part of the pole is then equal to the sum of the masses of the decay products, weighted by the branching ratios for the particular decay channel. In analogy to this consideration we now define an "effective flux loop mass" by the sum of the masses of the 0^{++} eigenstates, weighted by their maximal overlap onto a Polyakov line operator,

$$\langle aE_F \rangle \equiv \frac{\sum_i \mid a_{PL,i} \mid^2 aM_i}{\sum_i \mid a_{PL,i} \mid^2} \ . \tag{15}$$

In the same manner we construct the average square of the flux loop energy, $\langle E_F^2 \rangle$. From these we then obtain the "width" of the flux loop as the root mean square fluctuation

$$(a\Gamma_F)^2 = \langle (aE_F)^2 \rangle - \langle aE_F \rangle^2 \ . \tag{16}$$

These two quantities are plotted through the crossover region in Fig. 8. Indeed, the decay width defined in this way is nearly zero on the confinement side and then increases smoothly as it approaches the critical coupling. It then maintains its higher value on the Higgs side indicating the instability and non-existence of flux loops on this side of the transition.

We conclude that, although the spectra are very similar on both sides of the critical β_H^c for large scalar coupling, we have clear evidence for a pronounced change in the
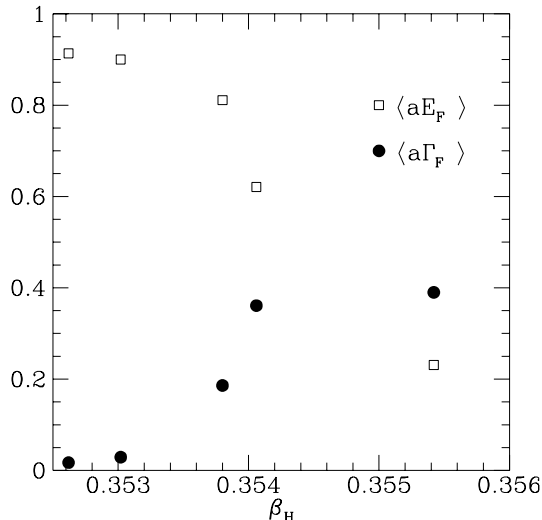
Figure 8: *Effective energy and decay width of the flux loop for the decay into single particle 0^{++} states.*

dynamics as one moves from the confining to the Higgs region. In particular it is possible to demonstrate the growing instability of flux loops through the transition. We remark, however, that the concept of a flux loop only exists in a finite volume, and thus this analysis does not have an infinite-volume limit. Nevertheless we would expect the same phenomena to happen if one were to investigate the physical flux tube between two static external charges at a given separation and then change the parameters from the confining regime to the Higgs regime.

7   Summary and conclusions

In this paper we have extended our previous work on the $(2 + 1)$-dimensional SU(2) gauge-fundamental Higgs model in various ways. Firstly, we have added the 2^{++} mass spectrum to our previous calculations of the 0^{++} and 1^{--} spectra. Secondly we have added operators based on Polyakov loops. If we have confinement then these loops will project onto chromoelectric flux loops ("torelons") that close through one of the periodic spatial boundaries. In that case the lightest mass extracted from the correlation function of such an operator will be proportional to the lattice spatial size, and its mass density will give the confining string tension (up to corrections, the leading one of which is universal and known). This allows us to probe directly the confining properties of the

theory at various points in the phase diagram. At the same time we have extended our basis of operators in the mass spectrum calculations; in part by the inclusion of these torelon operators and also products of them. This provides us with a much better control of finite-volume effects. We have in addition performed the calculations not only for the small scalar self-coupling at which our previous simulations were carried out, but also for a large value of the scalar coupling where no phase transition separates the symmetric and Higgs phases. Here we have performed calculations through the crossover region that separates these two phases. In all these calculations we have used only a single value of the inverse gauge coupling, but one for which our earlier calculations assure us that lattice corrections to the continuum limit are already small.

As well as extending our previous calculations, we have also shifted the emphasis of our physics interest away from the Electroweak Theory at finite temperature to dynamical phenomena that may be relevant to that other theory with gauge fields and charges in the fundamental representation: Quantum Chromodynamics.

So one major focus of our interest has been confinement. At small scalar self-coupling we find that the torelon mass increases (approximately) linearly with its length and hence that the symmetric phase is confining. Of course we know that, just as in QCD, flux tubes will be broken through the pair creation of fundamental charges, but within our errors we see no sign of this. The string tension is almost identical to its pure gauge value. By contrast, in the Higgs phase, we see what perturbation theory tells us to expect: the Polyakov loop operator couples to a WW-scattering state instead of to the now non-existent flux tube. Indeed, apart from the Higgs scalar, WW-scattering states are all we see in the 0^{++} and 2^{++} spectra. More intriguing is the situation for large scalar self-coupling. Here we once again have a symmetric phase that is almost confining and a Higgs phase that is not at all confining. However, now there is no first-order transition between the two phases, only a smooth crossover. This raises the question of how the dynamics can smoothly interpolate between the two phases. We provided evidence for the following picture. In the pure gauge theory a flux loop joined upon itself through a boundary is a stable state (of the finite volume Hamiltonian). With fundamental charges present such a state can decay. Far from the crossover such decays are strongly suppressed and the flux loop will be almost stable: a resonance with a very narrow decay width. As we enter the crossover region the decay width becomes rapidly larger: so the pole in the complex energy plane moves rapidly away from the real axis. As (initially) a secondary effect, the real part will also change, because of the newly enhanced intermediate states, and so the mass will shift as well. At some point, near the centre of the crossover, the

pole is so far from the real axis that one completely loses a particle interpretation. At this point it is no longer useful to talk of confining flux tubes. We have found it convenient to use a periodic flux loop on a finite volume as a probe of confinement, but one can clearly use a finite flux line between fundamental sources/charges equally well.

Our second major interest has been the approximate decoupling between scalar and gauge degrees of freedom which we observed in our previous work. There we found that in the symmetric phase there are states which are almost entirely gluonic and the masses of these states coincide with the glueball masses of the pure gauge theory. We now find that this occurs not only in the 0^{++} sector, but also in the 2^{++} sector, and at large scalar self-coupling as well as at small. Moreover this phenomenon only gradually disappears as we move through the crossover to the Higgs phase. Indeed, there is some evidence that a remnant of this phenomenon survives even in the Higgs phase. Amongst other things this tells us that the mixing between glueballs and states composed of fundamental charges is strongly suppressed, at least as long as we have some remnant of linear confinement. It also tells us that this is a very robust phenomenon. Is it robust enough to extend to QCD? There it would support the idea that glueball-quarkonium mixing should be suppressed and that we should search experimentally for glueballs at the masses found in the corresponding pure gauge theory. These are important questions but we need some understanding of the underlying dynamics if we are to move beyond the realm of conjecture.

In addition to the above two topics, we also clarified the unusually strong finite-volume effects that we saw in our previous work. It turns out that these are operator artefacts. In fact, the true bound states show weak finite volume effects. However, if one uses smeared operators it is difficult to avoid components that are essentially (smeared) Polyakov loops. These components introduce the torelon into the measured spectrum and, of course, the mass of this varies rapidly with volume. This is a generic problem when one has a theory with fundamental charges, and the simplest way to deal with it is to include smeared torelon operators in the operator basis. After diagonalisation one can explicitly determine which states have dominant torelon components.

Finally we point to the dense spectrum of states we have found in the Higgs phase at large scalar coupling. This is in a phase without confinement, and presumably the dynamics is not being driven by the gauge coupling becoming large at large distances. It is therefore tempting to conclude that what we have here is a generic example of a spectrum produced by a strong scalar self-coupling.

We conclude with a brief comment as to how these calculations need to be improved.

The most obvious lacuna concerns multiparticle scattering states. We have not attempted to identify these, except in the very obvious case of the Higgs phase at small scalar self-coupling. There is some evidence that our operators, which are naively designed to project only onto single particle states, usually do so. However, this really needs to be checked explicitly, especially in the strong-coupling Higgs phase where, if it turns out not to be the case, it could completely alter our interpretation of the spectrum. The inclusion of scattering states is also necessary if we are to perform a proper analysis of flux tube decay through the crossover region. Technically the problem is simple. For example, suppose $\phi(\vec{p}, t)$ is an operator that has a very good projection onto the lightest scalar with momentum $\vec{p}$ (which will be one of the discrete set of allowed momenta in our finite volume). Then the operator $\phi_2(t) \equiv \phi(+\vec{p}, t)\phi(-\vec{p}, t)$ (vacuum subtracted if necessary) will be a good operator for the two-scalar scattering state of zero total momentum and finite relative momentum. At least this will be so for volumes that are not too small. In similar ways one can build other trial multiparticle operators and add them to the operator basis. However, to be confident that one is correctly isolating multiparticle states one needs to do an accurate finite volume analysis that shows the continuum cut gradually forming as one increases the volume. This would be a substantially larger calculation than the one in this paper. It would also be very interesting to further pursue the scalar-glue decoupling; in particular to see if it might be related to the OZI rule in QCD.

References

[1] K. Kajantie, M. Laine, K. Rummukainen and M. Shaposhnikov, Nucl. Phys. B466 (1996) 189.

[2] K. Kajantie, M. Laine, K. Rummukainen and M. Shaposhnikov, Phys. Rev. Lett. 77 (1996) 2887.

[3] E.M. Ilgenfritz, J. Kripfganz, H. Perlt and A. Schiller, Phys. Lett. B356 (1995) 561;
M. Gürtler, E.M. Ilgenfritz, J. Kripfganz, H. Perlt and A. Schiller, Nucl. Phys. B83 (1997) 383;
M. Gürtler, E.M. Ilgenfritz and A. Schiller, hep-lat/9702020; Phys. Rev. D56 (1997) 3888.

[4] O. Philipsen, M. Teper and H. Wittig, Nucl. Phys. B469 (1996) 445.

[5] F. Karsch, T. Neuhaus and A. Patkós, Nucl. Phys. B442 (1995) 629;
F. Karsch, T. Neuhaus, A. Patkós and J. Rank, Nucl. Phys. B474 (1996) 217.

[6] P. Ginsparg, Nucl. Phys. B 170 (1980) 388; T. Appelquist and R. Pisarski, Phys. Rev. D 23 (1981) 2305; K. Kajantie, M. Laine, K. Rummukainen and M. Shaposhnikov, Nucl. Phys. B 458 (1996) 90; A. Jakovác and A. Patkós, Nucl. Phys. B 494 (1997) 54.

[7] F. Csikor, Z. Fodor, J. Hein, J. Heitger, A. Jaster and I. Montvay, Nucl. Phys. B (Proc. Suppl.) 53 (1997) 612.

[8] W. Buchmüller and O. Philipsen, Nucl. Phys. B443 (1995) 47.

[9] E. Fradkin and S. Shenker, Phys. Rev. D19 (1979) 3682.

[10] K. Rummukainen, Nucl. Phys. B (Proc. Suppl.) 53 (1997) 30.

[11] H.-G. Dosch, J. Kripfganz, A. Laser and M. G. Schmidt, Phys. Lett. B365 (1996) 213; HD-THEP-96-53, hep-ph/9612450.

[12] W. Buchmüller and O. Philipsen, Phys. Lett. B397 (1997) 112.

[13] O. Philipsen, M. Teper and H. Wittig, Nucl. Phys. B (Proc. Suppl.) 53 (1997) 626.

[14] O. Philipsen, presented at Eötvös Conference in Science: Strong and Electroweak Matter (SEWM 97), Eger, Hungary, 21-25 May 1997, hep-ph/9708309.

[15] M. Gürtler, E.M. Ilgenfritz, A. Schiller and C. Strecha, presented at 15th International Symposium on Lattice Field Theory, "Lattice 97", Edinburgh, Scotland, 22-26 Jul 1997, hep-lat/9709020.

[16] M. Laine, Nucl. Phys. B451 (1995) 484.

[17] M. Teper, Phys. Lett. B187 (1987) 345.

[18] M. Albanese et al., Phys. Lett. B192 (1987) 163; Phys. Lett. B197 (1987) 400.

[19] H. Wittig, Nucl. Phys. B325 (1989) 242.

[20] C. Michael, J. Phys. G13 (1987) 1001.

[21] K. Fabricius and O. Haan, Phys. Lett. B143 (1984) 459.

[22] A.D. Kennedy and B.J. Pendleton, Phys. Lett. B156 (1985) 393.

[23] B. Bunk, Nucl. Phys. B (Proc. Suppl.) 42 (1995) 566.

[24] I. Montvay and P. Weisz, Nucl. Phys. B290 (1987) 327.

[25] P. de Forcrand G. Schierholz, H. Schneider and M. Teper, Phys. Lett. 160B (1985) 137.

[26] M. Teper, unpublished.

[27] M. Teper, Phys. Lett. B311 (1993) 223.

[28] W. Buchmüller and Z. Fodor, Phys. Lett. B331 (1994) 131.